Spatiotemporal transformation of dissolved organic matter along an alpine stream flowpath on the Qinghai-Tibetan Plateau: importance of source and permafrost degradation

Yinghui Wang [a,b], Robert G.M. Spencer [c], David C. Podgorski [d], Anne M. Kellerman [c], Harunur Rashid [a], Phoebe Zito [d], Wenjie Xiao [b], Dandan Wei [a], Yuanhe Yang [e], Yunping Xu [a*]

[a] *Shanghai Engineering Research Center of Hadal Science and Technology*, *College of Marine Sciences, Shanghai Ocean University, Shanghai 201306, China.*

[b] *Key Laboratory for Earth Surface Processes of the Ministry of Education, College of Urban and Environmental Sciences, Peking University, Beijing 100871, China.*

[c] *National High Magnetic Field Laboratory Geochemistry Group and Department of Earth, Ocean, and Atmospheric Science, Florida State University, Tallahassee, FL 32306, USA*

[d] *Pontchartrain Institute for Environmental Sciences, Department of Chemistry, University of New Orleans, New Orleans, LA, 70148, USA*

[e] *State Key Laboratory of Vegetation and Environmental Change, Institute of Botany, Chinese Academy of Sciences, Beijing 100093, China*

*Corresponding author. *E-mail*: ypxu@shou.edu.cn (Y. Xu)

Abstract The Qinghai-Tibetan Plateau (QTP) accounts for approximately 70% of global alpine permafrost and is an area sensitive to climate change. The thawing and mobilization of ice and organic carbon-rich permafrost impact hydrologic conditions and biogeochemical processes on the QTP. Despite numerous studies of Arctic permafrost, there are no reports to date for the molecular-level in-stream processing of permafrost-derived dissolved organic matter (DOM) on the QTP. In this study, we examine temporal and spatial changes of chemical composition of DOM and ^{14}C age of dissolved organic carbon (DOC) along an alpine stream (3850–3207 m above sea level) by Fourier transform ion cyclotron resonance mass spectrometry (FT-ICR MS), accelerator mass spectrometry (AMS) and UV-visible spectroscopy. Compared to downstream sites, the DOM at the headstream exhibited older radiocarbon (^{14}C-DOC) age, higher mean molecular weight, higher aromaticity and fewer polyunsaturated components. At the molecular level, 6409 and 1345 formulas were identified as unique to the active layer (AL) leachate and permafrost layer (PL) leachate, respectively. Comparing permafrost leachates to the downstream site, 59% of AL-specific formulas and 90% of PL-specific formulas were degraded, likely a result of rapid instream degradation of permafrost-derived DOM. From peak discharge in the summer to low flow in late autumn, the DOC concentration at the headstream site decreased from 13.9 to 10.2 mg/L, while the ^{14}C-DOC age increased from 745 to 1560 years before present (BP), reflecting an increase in relative contribution of deep permafrost carbon due to the effect of changing hydrological conditions over the course of the summer on DOM source (AL vs. PL). Our study thus demonstrates that hydrological conditions impact the mobilization of permafrost carbon in an alpine fluvial network, the signature of which is quickly lost through instream mineralization and transformation.

Keywords: dissolved organic matter; permafrost; Qinghai-Tibet Plateau; FT-ICR MS;

radiocarbon age

1. INTRODUCTION

The amount of carbon stored in permafrost is roughly twice as much as that in the atmosphere and represents the largest component of the terrestrial carbon pool (Zimov et al., 2006; Tarnocai et al., 2009). Accelerated climate warming has led to a succession of changes associated with permafrost thaw, where liquid water once frozen in permafrost soils has changed watershed hydrology, topography and ecosystem biogeochemistry (Frey and Smith, 2005; Abbott et al., 2015; Vonk et al., 2015). When permafrost-derived carbon enters aquatic system, it can be rapidly mineralized and transformed by microbes and light (Cory et al., 2014; Drake et al., 2015; Vonk et al., 2015). Therefore, the mobilization of carbon from permafrost soils where it has been relatively stable for thousands of years into dissolved carbon could increase greenhouse gas emissions (Cory et al., 2013; Vonk et al., 2013; Mann et al., 2015; Ward and Cory, 2016; Selvam et al., 2017) and exacerbate climate warming via a positive feedback loop (Koven et al., 2011; Schuur et al., 2015).

The seasonal thawing-freezing cycle of permafrost soils could change hydrologic condition and restrict source water contributions to river flow, leading to variability in the flux and the chemical composition of dissolved organic matter (DOM) in permafrost-impacted watersheds (Petrone et al., 2006; Laudon et al., 2011). DOM in the Yukon River exhibits seasonal changes in aromaticity, molecular weight, ^{14}C age and biodegradability (Striegl et al., 2007; Spencer et al., 2008; Wickland et al., 2012; O'Donnell et al., 2014). Since the persistence of DOM in aquatic systems is related to chemical composition (Kellerman et al., 2015; Kellerman et al., 2018), substituting space for time to trace changes in DOM composition along a hydrologic flowpath may

illustrate the environmental behavior and fate of seasonally exported permafrost carbon.

The Qinghai-Tibet Plateau (QTP), the world's largest and highest plateau, plays a critical role in the evolution of the Asian Monsoon (Sato and Kimura, 2007; Wu et al., 2007) and supplies water to several large rivers such as the Yangtze River, Yellow River and Yarlung Tsangpo (Yao et al., 2007; Kang et al., 2010). As a climate sensitive region, the QTP has experienced significant warming since the 1950s (Qiu, 2008) with the mean annual air temperature rising at a rate of 0.36 °C per decade from 1961 to 2007 (Wang et al., 2008). Consequently, the permafrost soils on the QTP have begun to thaw and collapse, causing abundant carbon loss from degradation, leaching and lateral displacement (Mu et al., 2016). However, compared with an abundance of studies on Arctic permafrost, biogeochemical studies on QTP permafrost are scant (Mu et al., 2016). This results in a limited understanding of the permafrost carbon cycle as a whole since the QTP represents nearly 10% of the global permafrost, what's more, the QTP differs from the Arctic in altitude, climate, and hydrology (Bockheim and Munroe, 2014).

Here, we conducted a study on the spatial and temporal change of permafrost-derived DOM on the northeastern QTP. We applied multiple analytical techniques including Fourier transform ion cyclotron resonance mass spectrometry (FT-ICR MS), AMS radiocarbon (^{14}C), and UV-visible optical spectroscopy. Our objective is two-fold: 1) determine the dominant sources of alpine stream DOM on the QTP (active layer (AL) vs. permafrost layer (PL)), and 2) trace the persistence and degradation of permafrost-derived DOM in an alpine fluvial network. This work represents the first step in characterizing in-stream removal and transformation processes of permafrost carbon at the molecular level on the QTP.

2. MATERIALS AND METHODS

2.1. Study area and sampling

Our study area is located in Gangcha County, north of Qinghai Lake. The climate is typical plateau continental climate, characterized by extensive sunshine duration (~3000 hours per year), long cold and dry winters and short cool and humid summers (Peng et al., 2015). During 2013-2016, January had the lowest average monthly temperature (–11.82 °C), while December had the lowest average monthly precipitation (0.3 mm). Meanwhile, the highest average monthly temperature and precipitation occurred in July (11.66 °C) and August (124.67 mm), respectively. These climate data are available at http://data.cma.cn. The permafrost soil was developed in the late Quaternary, and accumulated > 2 m thick in mountainous areas of the Gangcha County. Due to the rapid climate warming on the QTP, the ice-rich permafrost began to thaw, and several thermo-erosion gullies formed a decade ago. In this study, we focused on a continuous system that starts with a thermo-erosion gully (> 200 m long), forms a stream which flows into Qinghai Lake, the largest lake in China with a surface area of ca. 4500 km^2. Thawed permafrost slumping exposed soil profiles at the gullies' head (ca. 3850 meters above sea level; masl). The top 60 cm is an active layer (AL) that comprises abundant grass litter and roots, underlain by a dark permafrost layer (PL) without visible plant debris. The thaw depth reached 78 cm in August 2015. Seasonal thaw of the entire AL and the upper PL allows for both vertical and lateral percolation of rainwater, which mobilizes large amounts of particulate and dissolved organic matter. The water in the gully flows southward across the hillslope before draining into Qinghai Lake, and the total length of the stream is around 40 km (Fig. 1).

Our fieldwork was conducted in the summer and autumn of 2015 and 2016. In 2015, a time-series sampling campaign was conducted at the headstream (Q-1) from August

120 1st when the warm and humid climate caused the largest export of leachates, to October
121 15th when the leaching ceased due to little precipitation and low temperature. On August
122 1st of 2016 and 2017, AL and PL leachates were collected at the depth of 60 cm and 220
123 cm, respectively, of the gullies' head. 20 L HDPE carboys were cleaned by pure water,
124 0.1 N hydrochloric acid and pure water prior to use. It usually took 2 days to gather >
125 15 L leaching waters. After that, the leachate samples were immediately kept on ice and
126 in the dark by aluminum foil. They were transported to the temporary laboratory in the
127 Gangcha County within 6 hours. Besides soil leachates, water samples (20 L each) were
128 collected from twenty sites along the stream (Fig. 1). Sampling sites Q-1 to Q-10 are
129 located in a first-order stream (ca. 8.5 km long) that originates in the largest thermo-
130 erosion gully, whereas sites Q-11 and Q-12 are located in another first-order stream
131 nearby (ca. 6.9 km long). These two streams merge together to form the main stream,
132 along which sampling sites Q-13 to Q-20 were located. Surface water samples were
133 collected using pre-cleaned HDPE carboys and kept on ice and in the dark until filtering
134 through Whatman GF/F filters (0.7 μm) within 6 hours after sampling. To obtain enough
135 carbon for ^{14}C analyses, aliquots of the 0.7 μm filtrate were concentrated over a cross-
136 flow ultrafiltration system with 1 kDa cut off (Millipore®, Pellicon 2 system). The
137 retentates and the remaining filtrate were all stored at –20 ºC until further analysis. All
138 glassware and GF/F filters were combusted at 450 ºC for at least 4 hours prior to use.
139
140 **2.2. Hydrological condition, DOC concentration and spectral absorbance in alpine**
141 **streams**
142 On Aug. 1st 2015, stream water temperature, pH and conductivity were measured
143 with a portable Horiba W-23XD Water Quality Monitoring System. The water flux was
144 calculated according to flow rate and cross-sectional area of the stream. The DOC

concentration of each water sample was determined by 3-5 injections on a Shimadzu TOC-V_{CPH} analyzer using high temperature combustion, and the coefficient of variance across measurements was < 2%.

The optical properties of the water samples were determined using a Shimadzu UV-1800 spectrophotometer. The scan range was between 200 and 800 nm and Milli-Q water (18.2 MΩ cm^{-1}) was used as the blank. A quartz cell with 1.0 cm path length was used. The spectral slope of the 275–295 nm region ($S_{275\text{-}295}$), an indicator for the molecular weight of DOM (Helms et al., 2008), was determined by applying log linear fits across the wavelengths 275–295 nm. Specific UV absorbance ($SUVA_{254}$), an indicator for relative aromatic C content, was calculated by dividing the decadic UV absorbance at 254 nm with DOC concentration (Weishaar et al., 2003).

2.3. Electrospray ionization Fourier transform ion cyclotron resonance mass spectrometry (ESI FT-ICR MS)

Selected water samples collected in 2016 from headstream (Q-1), mid-stream (Q-9), and downstream (Q-17), as well as leachate samples collected from the AL and PL, were prepared for FT-ICR MS analyses. They were solid-phase extracted (SPE) using the Bond Elut PPL (Agilent Technologies, 100 mg PPL in 3 ml cartridge), following the procedures of Dittmar et al. (2008). In order to avoid overloading of the SPE column, the aliquot volume of SPE DOM was calculated based on an average SPE recovery (60% for permafrost DOM; Ward et al., 2015) and a final eluate concentration of 40 μg C/ml (in 2 ml methanol). The methanol extracts were analyzed on a 9.4 Tesla custom-built FT-ICR MS at the National High Magnetic Field Laboratory (NHMFL; Tallahassee, FL; Kaiser et al., 2011). The injection speed was 0.7 μL/min. A total of 100 broadband scans was accumulated for each mass spectra. Other instrumental parameters can be found in

Hodgkins et al. (2016). After internal calibration in MIDAS Predator Analysis (NHMFL), formulas were assigned based on published rules to peaks with intensities > 6σ baseline noise (Stubbins et al., 2010) using EnviroOrg®™ software and categorized by compound class based on the elemental composition of molecular formulas (Kujawinski, 2002; Stenson et al. 2003; Spencer et al., 2014; Corilo, 2015). A modified aromaticity index (AI_{mod}) was calculated according to the definition of Koch and Dittmar (2006): $AI_{mod} = \frac{1+C-0.5O-S-0.5(H+N+P)}{C-0.5O-S-N}$, and if AI_{mod} is negative, then AI=0. The groups referenced in this study are: 1) aliphatics (Ali.): H/C 1.5 - 2.0, O/C < 0.9, N = 0; 2) peptides (Pep.): H/C 1.5 - 2.0, O/C < 0.9, N > 0; 3) highly unsaturated compounds (Uns.): AI_{mod} < 0.5, H/C < 1.5; 4) polyphenols (Pol.): 0.5 < AI_{mod} < 0.67; 5) condensed aromatics (CA): $AI_{mod} \geq 0.67$. The relative abundance of the defined compound class was weighted by signal magnitude in each spectrum.

2.4. Radiocarbon analyses

Freeze-dried retentates from ultrafiltration were fumigated with concentrated hydrochloric acid (12 M) in order to remove inorganic carbon. After that, the samples were analyzed on the Keck Carbon Cycle Accelerator Mass Spectrometry (AMS) Facility at the University of California, Irvine, USA. Processing blank and sample preparation backgrounds were subtracted. Radiocarbon concentrations are given as conventional ^{14}C age following Stuiver and Reimer (1993).

3. RESULTS

3.1. Hydrology and DOC concentration from headstream to downstream water

Discharge increased along the stream reach, from 0.15 m^3/min at the headstream (Q-1) on August 1st 2015 to 24.14 m^3 /min (Q-19) (Fig. 2). pH increased from 7.4 at Q-

1 to 8.2 at Q-4 and remained elevated in the middle and lower stream (7.9 to 8.4). Conductivity was relatively constant from Q-1 to Q-6 (35 to 38 μs/cm), then increased at Q-7 and remained elevated downstream (48 to 60 μs/cm). The DOC concentration was high in headstream waters (e.g., 11.69 ± 0.60 mg/L at Q-1 and 10.22 ± 1.09 mg/L at Q-2; Mean ± AD, same hereafter) and decreased downstream (3.29 ± 0.75 to 4.73 ± 0.21 mg/L from Q-5 to Q-20). The mean DOC concentration of the AL leachates (11.57 ± 0.77 mg/L) was an order of magnitude lower than that of the PL leachates (126.40 ± 14.80 mg/L).

3.2. Optical properties of DOM in leachates and stream waters

Paired t-test based on $S_{275\text{-}295}$ and $SUVA_{254}$ of water samples showed no significant inter-annual variation between year 2015 and 2016 ($p = 0.716$ and $p = 0.321$, respectively). The mean $S_{275\text{-}295}$ of 2015 and 2016 samples was $(14.49 \pm 0.34) \times 10^{-3}$ nm^{-1} for the AL leachates and $(18.05 \pm 0.94) \times 10^{-3}$ nm^{-1} for the PL leachates. In the stream waters, the $S_{275\text{-}295}$ ranged from 16.05×10^{-3} to 21.80×10^{-3} nm^{-1}, increasing in downstream reaches. The mean $SUVA_{254}$ was 3.53 ± 0.17L mg C^{-1} m^{-1} for the AL leachates and 0.95 ± 0.10L mg C^{-1} m^{-1} for the PL leachates, and decreased in the stream from Q-1 to Q-11 (2.92 to 1.66 L mg C^{-1} m^{-1}), and then remained low (Fig. 3). A strong negative correlation was found between $SUVA_{254}$ and $S_{275\text{-}295}$ for water samples from both years ($R^2 = 0.77$, $P < 0.01$).

3.3. Spatiotemporal change of ^{14}C-DOC age through fluvial networks

^{14}C-DOC age of the PL leachate was 4145 years BP, which was much older than that of the AL leachate (535 years BP; Fig. 4a). The ^{14}C-DOC age decreased along the stream from 745 years BP for the headstream water (Q-1) to 160 years BP at Q-19, a

site close to Qinghai Lake. Besides apparent spatial variability, the ^{14}C-DOC age also changed temporally. In 2015, the ^{14}C-DOC age of the headstream water (Q-1) increased from 745 years BP on August 1st, to 1015 years BP on August 11th and 1560 years BP on September 5th (Fig. 4b).

3.4. FT-ICR MS characterization of SPE-DOM

Compared with the PL leachate, the AL leachate was characterized by higher molecular chemodiversity (14709 vs. 9645 assigned formulae), higher mean molecular weight (498.81 vs. 452.73 Da) and higher AI_{mod} (0.47 vs. 0.30). Molecular-level composition revealed that compounds containing both N and S were only detected in the AL leachates and headstream waters. The AL leachate contained 54.28% highly unsaturated compounds, 27.10% polyphenols and 17.23% condensed aromatic compounds, whereas the proportion of aliphatics and peptides was minor (ca. 1.30%). Compared with the AL leachate, the PL leachate comprised a higher proportion of polyunsaturated compounds (74.23%) and aliphatics + peptides (10.04%), but a lower proportion of polyphenols (11.33%) and condensed aromatics (4.32%).

Along the stream (Q-1, Q-9, and Q-17), the molecular chemodiversity, mean molecular weight and modified aromaticity index of SPE-DOM decreased from 14924 to 11074, 510.1 to 486.5 Da and 0.43 to 0.36, respectively (Table 1). The relative abundance of aromatics (condensed aromatics and polyphenols) decreased by 48% (35.7% at Q-1 vs. 18.4% at Q-17), whereas that of highly unsaturated compounds increased by 28% (62.8% at Q-1 vs. 80.3% at Q-17). Aliphatics and peptides were minor components of stream DOM (<1.3%) and did not exhibit a downstream trend.

4. DISSCUSSION

4.1. AL leachates as a major source of stream DOM

The UV-visible optical parameters and molecular formulas resolved by FT-ICR MS show that the AL and PL leachates have different chemical compositions (Table 1 and 2). This difference is likely attributed to selective release of aromatic components from AL and carbohydrate/protein components from deep PL during the soil thawing process which was observed in our previous study (Wang et al., 2018). Since chemical composition impacts the reactivity of DOM (Kellerman et al., 2015), the differing chemical composition between the AL and PL leachates that enter the stream may influence bioavailability (Vonk et al., 2013) and photolability (Stubbins et al., 2017). Thus, distinguishing DOM source is crucial for understanding in-stream biogeochemical processes in permafrost-impacted systems. DOM may originate from a variety of sources including permafrost soil (AL and PL) leaching, in-situ microbial production, and wet deposition from snow and rain. At the headstream site (Q-1), however, the dominant source of DOM is permafrost soil leaching, as short residence times at the gully head restrict in-stream production and wet deposition is likely negligible due to low DOC concentrations in Tibetan glaciers (0.2-3.3 μg/ml; Spencer et al., 2014). Assuming that headstream DOM is derived only from permafrost soil leaching, we are able to estimate the relative contributions of DOM from the AL and PL.

The mean DOC concentration of the AL leachate based on samples from 2015 and 2016 (11.57 ± 0.77 mg/L) is similar to that of the headstream (Q-1; ca. 11.69 ± 0.60 mg/L), but substantially lower than that of the PL leachates (126.40 ± 14.80 mg/L), supporting a predominance of AL-leachate DOM in stream waters. In addition, the $SUVA_{254}$ is 3.52 ± 0.17 L mg C^{-1} m^{-1} for AL leachates and 0.95 ± 0.10 L mg C^{-1} m^{-1} for PL leachates, whereas the $S_{275\text{-}295}$ is (14.49 ± 0.34) × 10^{-3} nm^{-1} for AL leachates and

(18.05 ± 0.94) × 10^{-3} nm^{-1} for PL leachates. Similar optical properties and DOC concentrations between AL-leachates and the headstream water (3.52 ± 0.17 L mg C^{-1} m^{-1} vs 2.92 ± 0.13 L mg C^{-1} m^{-1} for $SUVA_{254}$ and (14.49 ± 0.34) × 10^{-3} nm^{-1} vs (16.05 ± 0.28) × 10^{-3} nm^{-1} for $S_{275\text{-}295}$) support DOM that leaches from the AL dominates stream DOM. Furthermore, the stream water at Q-1 has a ^{14}C-DOC age of 745 years BP, close to that of the AL leachate (535 years BP), and much younger than that of the PL leachate (4145 years BP). We estimate the portion of AL and PL-derived C by using a binary mixing model based on $\Delta^{14}C$ values of bulk DOC (Criss, 1999):

$$\Delta^{14}C_{DOM} = f_{AL} \times \Delta^{14}C_{AL} + f_{PL} \times \Delta^{14}C_{PL}$$

$$1.0 = f_{AL} + f_{PL}$$

According to this model, ca. 94% of DOC collected from stream site Q-1 on Aug. 1, 2015 originated from the AL (Fig. 6a). Headstream ^{14}C-DOC age increased from summer to fall (Fig. 4b), reflecting an enhanced contribution of old carbon from the deeper soils (i.e., PL), however, the AL still accounted for ≥ 72% of total DOC exported (Fig. 6a). This binary mixing model may overestimate the contribution of AL to stream DOC since PL-derived DOC may be degraded faster than AL-derived DOC, due to the high biolability of ancient permafrost carbon as shown in Arctic ecosystems (Vonk et al., 2013). Nonetheless, the AL appears as a major contributor to stream DOC in the QTP.

Seasonal variation of ^{14}C-DOC (Fig. 4b) has been previously observed in high latitude permafrost areas in Alaska (Aiken et al., 2014; O'Donnell et al., 2014), with the most enriched ^{14}C values observed in the spring and becoming more depleted through summer-fall and/or during winter. Our result also shows seasonal variations in ^{14}C age and optical parameters of headstream DOM. From summer to fall, the $SUVA_{254}$ of stream DOM at Q-1 decreased from 2.79 to 2.36 mg C^{-1} m^{-1}, whereas the $S_{275\text{-}295}$

295 increased from 16.33 × 10^{-3} to 16.96 × 10^{-3} nm^{-1}. These temporal changes indicated that
296 the proportion of aromatic components and high molecular weight compounds
297 decreased with the deepening of permafrost thawing. The mean monthly air temperature
298 of Gangcha County, after reaching the maximum in July (ca. 10.5 ºC), decreases to 2.1
299 ºC in September (data from http://data.cma.cn). As air temperature drops, surface soils
300 freeze earlier than deeper soils, leading to an increase in the relative contribution of
301 deep soil carbon (i.e. PL) to stream DOM, although the DOC concentration in Q-1
302 decreased from 13.87 mg/L to 10.22 mg/L (Fig. 6b).
303
304 **4.2. Selective removal of DOM along the alpine stream on the QTP**
305 The DOC concentration decreased (11.69 to 3.29 mg/L) from upper to mid-stream
306 (Q-1 to Q-5), which could be attributed to a dilution effect and/or in-stream degradation
307 of DOM. Dilution from groundwater is likely since groundwater discharge sustains
308 baseflow of rivers and streams in the QTP (Ge et al., 2008). Downstream groundwater
309 inputs were further supported by the order of magnitude increase in discharge (1.49 to
310 24.14 m^3/min) and increase in conductivity (37 to 60 μs/cm). Moreover, downstream
311 DOC concentrations remained about 3.0-4.0 mg/L (Q-15 to Q-20), indicative of the low
312 DOC concentrations of groundwater. Conversely, a tributary that originated from
313 another thermo-erosion gully merged into the study stream, however, the different
314 tributaries exhibited similar DOC concentrations (e.g., Q-9 and Q-10 vs. Q-11 and Q-
315 12; Fig. 2d). The similarities in DOC concentrations were attributed to homogeneity in
316 dominant vegetation, soil type and climate, and thus, homogeneity in DOM inputs to
317 the different tributaries in our study area. Therefore, additional tributaries could not
318 explain the spatial pattern of DOC concentration.
319 Despite evident dilution, DOC attenuation could be partly due to in-stream

degradation given several lines of evidence from optical properties, radiocarbon age and molecular composition. The UV-visible optical parameters, $S_{275\text{-}295}$ and $SUVA_{254}$, have been widely used to reveal mean molecular weight and aromaticity of DOM, respectively (Weishaar et al., 2003; Helms et al., 2008; Spencer et al., 2009; Mann et al., 2012). A downstream increase for $S_{275\text{-}295}$ regardless of sampling time (Fig. 3a) reflects selected degradation of high molecular weight compounds, leading to the enrichment of low molecular weight DOM. In addition to $S_{275\text{-}295}$, $SUVA_{254}$ varied from 1.50 to 2.92 L mg C^{-1} m^{-1}, showing a general decrease downstream (Fig. 3b). Lignin, an aromatic biopolymer specific for vascular plants (Hedges et al., 1997), is relatively resistant to biodegradation (Hedges et al., 1985), but highly photo-labile (Lanzalunga and Bietti, 2000). Cory et al. (2014) found that sunlight accounts for 70% to 95% of water column carbon processing in Arctic rivers and lakes. Given strong solar radiation and long sunshine duration (~3000 hours per year) on the QTP (Peng et al., 2015), photo-degradation could be an important pathway for carbon removal in QTP streams. A strong negative correlation between $S_{275\text{-}295}$ and $SUVA_{254}$ ($R^2 = 0.73$, $p < 0.01$) indicates that photodegradation of high molecular weight aromatic compounds (like lignin) may play a role in the decrease of mean molecular weight of DOM along the stream, despite that microbial degradation might also contribute the molecular modification in stream.

Similar to $SUVA_{254}$ and $S_{275\text{-}295}$, the data from FT-ICR MS also show a downstream decrease in aromaticity (AI_{mod}: 0.43 to 0.36) and mean molecular weight of stream DOM (510.0 to 486.5 Da; Table 1). Compared with headstream DOM at Q-1, DOM at Q-9 and Q-17 was characterized by a lower proportion of condensed aromatics and polyphenols and enriched in highly unsaturated compounds (Table 1). The decrease in relative abundance of aromatic compounds is consistent with the reports for the

345 photolability of aromatic formulas within permafrost, river and ocean DOM (Stubbins
346 and Dittmar, 2015; Stubbins et al., 2017).

347 As discussed in section 4.1, AL is the principal contributor to stream DOM. Thus,
348 tracing AL-derived DOM is paramount in estimating biogeochemical processes of
349 carbon in the stream. FT-ICR MS identified 6409 molecular formulas specific to AL-
350 leachates (i.e. not observed in the PL, Table 2). Through various stream processes, some
351 AL specific formulas were removed from the DOM pool (from 17% by Q-1 up to 59%
352 by Q-17), which accounted for 66% of the aromatic compounds and 51% of the highly
353 unsaturated compounds (Table 2). Molecular formulas containing N and/or S were more
354 labile in the fluvial networks than CHO formulas, with 84% of S-containing formulas
355 and 100% of S and N-containing formulas lost (Table 2). Furthermore, the removal of
356 DOM formulas (ca. 83% of AL-specific formulas, and >95% of AL-specific formulas)
357 occurred in upper and mid-stream (leachates to Q-9). Concurrent with the rapid loss of
358 AL-specific formulas, some new molecular formulas were detected by FT-ICR MS,
359 which was mainly attributed to in-situ production by stream algae/microbes, an import
360 from groundwater and molecular transformation of leachate DOM. The van Krevelen
361 diagram showed that the new products were mainly composed of highly unsaturated
362 molecules (Fig. S1). The addition of new molecular formulas was also reflected by the
363 ^{14}C enrichment in middle and lower-stream (Fig. 3b).

364 Overall, our multiple analyses demonstrate a rapid and selective degradation of
365 stream DOM on the QTP. The attenuation of aromatic compounds and enrichment of
366 highly unsaturated compounds could change the environmental photo- and bio-lability
367 of DOM, increasing relative importance of photodegradation in upper stream and
368 biodegradation in lower stream. The continuous change in chemical properties of DOM
369 along the alpine stream flowpath has a potential to shift the aquatic microbial

community since DOM serves as an important energy and nutrient source(Wild et al., 2014).

4.3. Prediction of in stream carbon dynamic under continued warming

The DOC concentrations, UV-visible optical parameters and FT-ICR MS all suggest that currently, PL is a minor source to stream DOM (see 4.1). However, the QTP is a sensitive area to global warming, with a rate of air temperature rise that is approximately three times the global warming rate (Qiu, 2008). According to climate model predictions, spatial average temperatures of the QTP will increase by 0.68–0.98 ^{o}C for the period of 2015–2050 (Zhu et al., 2013), and in 2050, the mean AL thickness on the QTP permafrost will increase by approximately 0.3-0.8 m more than that in 2010 (Zhang and Wu, 2012). With the deepening of the AL, carbon that is currently stable in the PL will be thawed and mobilized into the downslope aquatic environments, which inevitably changes the proportion of AL vs. PL contributions to stream DOM. Thus, it is worth to trace chemical change of PL leachates along the stream. The PL leachate contained only 1345 formulas unique to the PL leachate in comparison to the AL, accounting for 14% of total assigned formulas (Table 2). Most PL-specific formulas were more biolabile components, e.g. aliphatics and peptides (73%), followed by highly unsaturated formulas (23.6%) and aromatics (1.9%). At the downstream site (i.e., Q-17), 90% of these PL-specific molecular formulas were lost, substantially higher than that of AL-specific formulas (59%). Furthermore, the vast majority of PL-specific formulas were lost within < 1 km (Q-1: 83%) whereas only 17% of AL-specific formulas were lost by Q-1 (Table 2). Therefore, the FT-ICR MS data demonstrate that permafrost thaw can trigger a rapid degradation of old carbon that was frozen in soils for thousands of years (Fig. 3a). This is consistent with findings in Arctic fluvial

networks that show the utilization of ancient permafrost carbon in headstream waters was rapid (Mann et al., 2015; Frey et al., 2016). Therefore, we hypothesize that with enhanced leaching of deep soil C under continued warming on the QTP, DOM in alpine streams will be more enriched in biolabile aliphatics/peptides and depleted in photolabile aromatics

Finally, despite substantial in-stream degradation, some old permafrost-derived carbon (i.e., polyphenols and highly unsaturated compounds) could persist downstream. In addition, CO_2 produced by respiration of old DOC could be utilized by stream algae to biosynthesize new DOM with an old carbon age. These effects resulted in a sustained deviation from modern ^{14}C-DOC age in the alpine stream (e.g., 160 years BP at Q-19), and were even detected in large rivers on the QTP (e.g., Yangtze River and Yellow River; Qu et al., 2017). Thus, under continued warming, a greater quantity of older C may be transported into large watersheds on the QTP, and thereby exert an important role in biogeochemical cycles there since older carbon has different photo and bio-lability from young carbon in AL soils.

5. CONCLUSIONS

Permafrost thaw represents positive feedbacks to climate change, but its carbon alteration and removal mechanism is not well known, particularly for the alpine permafrost such as the QTP. Here we use multiple analytical methods (e.g., FT-ICR MS, radiocarbon and UV-visible spectroscopy) to trace spatial and temporal variability of permafrost DOM along an alpine stream in the northeastern QTP, from which four conclusions have been reached.

1) Presently, the AL is the major source to stream DOM with relatively high aromaticity. This character, combined with strong solar radiation on the QTP, suggests

sunlight may be an important driver for DOM removal in alpine fluvial networks, which was corroborated by an almost 60% loss of AL specific formulas from the thermo-erosion gully head to downstream waters.

2) From summer to fall (seasonal permafrost thawing to freezing cycle), the concentrations and chemical composition of stream DOM varied significantly at the thermo-erosion gully head. Even though the total amount of the leached DOC decreased, the contribution of deep permafrost carbon with lower aromaticity and lower MW increased, reflected by an increase of ^{14}C-DOC age and a decrease in aromaticity of DOM.

3) Although both the AL and PL leachate DOM underwent rapid degradation in the alpine stream, some components with old ^{14}C-DOC age (mainly highly unsaturated) were recalcitrant to degradation and could be transported downstream, causing ^{14}C-DOC values that were more depleted than modern radiocarbon age downstream in our study, and even in large watersheds as observed in Qu et al. (2017).

4) With deepening of the AL under continued climate warming on the QTP, currently stable PL soils will thaw and release greater amounts of old, aliphatic/peptide-rich DOM to downstream waters. This change in source and chemical composition will make microbial degradation more important for carbon removal and may shift downstream microbial communities, even in large watershed systems. All these factors should be taken into account when interpreting alpine permafrost carbon dynamics under the amplified climate warming trend on the QTP.

ACKNOWLEDGEMENTS

This work was financially supported by the National Basic Research Program of China (2014CB954001). Y.W. thanks the China Scholarship Council for supporting

445 study in the United States of America as a joint Ph. D. student. We thank Futing Liu,
446 Yanyan Yan, Shangzhe Zhou, Xinyu Zhang for assistance in the field. FT-ICR MS was
447 supported by NSF (DMR-1157490).
448
449
450 **References**
451 Abbott, B.W., Jones, J.B., Godsey, S.E., Larouche, J.R. and Bowden, W.B. (2015)
452 Patterns and persistence of hydrologic carbon and nutrient export from collapsing
453 upland permafrost. Biogeosciences 12, 3725-3740.
454 Aiken, G.R., Spencer, R.G.M., Striegl, R.G., Schuster, P.F. and Raymond, P.A. (2014)
455 Influences of glacier melt and permafrost thaw on the age of dissolved organic carbon
456 in the Yukon River basin. Global Biogeochem. Cycles 28, 525-537.
457 Bockheim, J.G. and Munroe, J.S. (2014) Organic Carbon Pools and Genesis of Alpine
458 Soils with Permafrost: A Review. Arct. Antarct. Alp. Res. 46, 987-1006.
459 Corilo, Y.E. (2015) EnviroOrg. Florida State University.
460 Cory, R.M., Crump, B.C., Dobkowski, J.A. and Kling, G.W. (2013) Surface exposure
461 to sunlight stimulates CO_2 release from permafrost soil carbon in the Arctic. Proc. Natl.
462 Acad. Sci. USA 110, 3429-3434.
463 Cory, R.M., Ward, C.P., Crump, B.C. and Kling, G.W. (2014) Sunlight controls water
464 column processing of carbon in arctic fresh waters. Science 345, 925-928.
465 Criss, R.E. (1999) Principles of stable isotope distribution. Oxford University Press,
466 New York.
467 Dittmar, T., Koch, B., Hertkorn, N. and Kattner, G. (2008) A simple and efficient
468 method for the solid-phase extraction of dissolved organic matter (SPE-DOM) from
469 seawater. Limnol. Oceanogr. Methods 6, 230-235.

Drake, T.W., Wickland, K.P., Spencer, R.G., McKnight, D.M. and Striegl, R.G. (2015) Ancient low-molecular-weight organic acids in permafrost fuel rapid carbon dioxide production upon thaw. Proc. Natl. Acad. Sci. USA 112, 13946-13951.

Frey, K.E. and Smith, L.C. (2005) Amplified carbon release from vast West Siberian peatlands by 2100. Geophys. Res. Lett. 32, doi: 10.1029/2004GL022025.

Frey, K.E., Sobczak, W.V., Mann, P.J. and Holmes, R.M. (2016) Optical properties and bioavailability of dissolved organic matter along a flow-path continuum from soil pore waters to the Kolyma River mainstem, East Siberia. Biogeosciences 13, 2279-2290.

Ge, S., Wu, Q.B., Lu, N., Jiang, G.L. and Ball, L. (2008) Groundwater in the Tibet Plateau, western China. Geophys. Res. Lett. 35, 80-86.

Hedges, J.I., Cowie, G.L., Ertel, J.R., James Barbour, R. and Hatcher, P.G. (1985) Degradation of carbohydrates and lignins in buried woods. Geochim. Cosmochim. Acta 49, 701-711.

Hedges, J.I., Keil, R.G. and Benner, R. (1997) What happens to terrestrial organic matter in the ocean? Org. Geochem. 27, 195-212.

Helms, J.R., Stubbins, A., Ritchie, J.D., Minor, E.C., Kieber, D.J. and Mopper, K. (2008) Absorption spectral slopes and slope ratios as indicators of molecular weight, source, and photobleaching of chromophoric dissolved organic matter. Limnol. Oceanogr. 53, 955-969.

Hodgkins, S.B., Tfaily, M.M., Podgorski, D.C., Mccalley, C.K., Saleska, S.R., Crill, P.M., Rich, V.I., Chanton, J.P. and Cooper, W.T. (2016) Elemental composition and optical properties reveal changes in dissolved organic matter along a permafrost thaw chronosequence in a subarctic peatland. Geochim. Cosmochim. Acta 187, 123-140.

Kaiser, N.K., Quinn, J.P., Blakney, G.T., Hendrickson, C.L. and Marshall, A.G. (2011) A novel 9.4 tesla FTICR mass spectrometer with improved sensitivity, mass resolution,

and mass range. J. Am. Soc. Mass Spectrom. 22, 1343-1351.

Kang, S., Xu, Y., You, Q., Flügel, W.-A., Pepin, N. and Yao, T. (2010) Review of climate and cryospheric change in the Tibetan Plateau. Environ. Res. Lett. 5, doi:10.1088/1748-9326/1085/1081/015101.

Kellerman, A.M., Guillemette, F., Podgorski, D.C., Aiken, G.R., Butler, K.D. and Spencer, R.G.M. (2018) Unifying Concepts Linking Dissolved Organic Matter Composition to Persistence in Aquatic Ecosystems. Environ. Sci. Technol., doi: 10.1021/acs.est.1027b05513.

Kellerman, A.M., Kothawala, D.N., Dittmar, T. and Tranvik, L.J. (2015) Persistence of dissolved organic matter in lakes related to its molecular characteristics. Nat. Geosci. 8, 454-457.

Koch, B.P. and Dittmar, T. (2006) From mass to structure: an aromaticity index for high-resolution mass data of natural organic matter. Rapid Commun. Mass Spectrom. 20, 926-932.

Koven, C.D., Ringeval, B., Friedlingstein, P., Ciais, P., Cadule, P., Khvorostyanov, D., Krinner, G. and Tarnocai, C. (2011) Permafrost carbon-climate feedbacks accelerate global warming. Proc. Natl. Acad. Sci. U. S. A. 108, 14769-14774.

Kujawinski, E.B., (2002). Electrospray ionization fourier transform ion cyclotron resonance mass spectrometry (ESI FT-ICR MS): Characterization of complex environmental mixtures. Environ. Forensics 3, 207-216.

Lanzalunga, O. and Bietti, M. (2000) Photo- and radiation chemical induced degradation of lignin model compounds. J. Photochem. Photobiol. B: Biol. 56, 85-108.

Laudon, H., Berggren, M., Ågren, A., Buffam, I., Bishop, K., Grabs, T., Jansson, M. and Köhler, S. (2011) Patterns and dynamics of dissolved organic carbon (DOC) in boreal streams: the role of processes, connectivity, and scaling. Ecosystems 14, 880-

520 893.
521 Mann, P.J., Davydova, A., Zimov, N., Spencer, R.G.M., Davydov, S., Bulygina, E.,
522 Zimov, S. and Holmes, R.M. (2012) Controls on the composition and lability of
523 dissolved organic matter in Siberia's Kolyma River basin. J. Geophys. Res. Biogeosci.
524 117, doi:10.1029/2011jg001798.
525 Mann, P.J., Eglinton, T.I., McIntyre, C.P., Zimov, N., Davydova, A., Vonk, J.E., Holmes,
526 R.M. and Spencer, R.G. (2015) Utilization of ancient permafrost carbon in headwaters
527 of Arctic fluvial networks. Nat. Commun. 6, doi:10.1038/ncomms8856.
528 Mu, C., Zhang, T., Zhang, X., Li, L., Guo, H., Zhao, Q., Cao, L., Wu, Q. and Cheng, G.
529 (2016) Carbon loss and chemical changes from permafrost collapse in the northern
530 Tibetan Plateau. J. Geophys. Res. Biogeosci. 121, doi:10.1002/2015JG003235.
531 O'Donnell, J.A., Aiken, G.R., Walvoord, M.A., Raymond, P.A., Butler, K.D.,
532 Dornblaser, M.M. and Heckman, K. (2014) Using dissolved organicmatter age and
533 composition to detect permafrost thaw in boreal watersheds of interior Alaska. J.
534 Geophys. Res. Biogeosci. 119, 2155-2170.
535 Peng, S., Du, Q., Wang, L., Lin, A. and Hu, B. (2015) Long-term variations of
536 ultraviolet radiation in Tibetan Plateau from observation and estimation. Int. J. Climatol.
537 35, 1245-1253.
538 Petrone, K.C., Jones, J.B., Hinzman, L.D. and Boone, R.D. (2006) Seasonal export of
539 carbon, nitrogen, and major solutes from Alaskan catchments with discontinuous
540 permafrost. J. Geophys. Res. Biogeosci. 111, doi:10.1029/2006JG000281.
541 Qiu, J. (2008) The third pole. Nature 454, 393-396.
542 Qu, B., Sillanpää, M., Li, C., Kang, S., Stubbins, A., Yan, F., Aho, K.S., Zhou, F. and
543 Raymond, P.A. (2017) Aged dissolved organic carbon exported from rivers of the
544 Tibetan Plateau. PLoS One 12, e0178166, doi:

545 0178110.0171371/journal.pone.0178166.
546 Sato, T. and Kimura, F. (2007) How does the Tibetan Plateau affect the transition of
547 Indian monsoon rainfall? Mon. Weather Rev. 135, 2006-2015.
548 Schuur, E.A.G., McGuire, A.D., Schadel, C., Grosse, G., Harden, J.W., Hayes, D.J.,
549 Hugelius, G., Koven, C.D., Kuhry, P., Lawrence, D.M., Natali, S.M., Olefeldt, D.,
550 Romanovsky, V.E., Schaefer, K., Turetsky, M.R., Treat, C.C. and Vonk, J.E. (2015)
551 Climate change and the permafrost carbon feedback. Nature 520, 171-179.
552 Selvam, B.P., Lapierre, J.-F., Guillemette, F., Voigt, C., Lamprecht, R.E., Biasi, C.,
553 Christensen, T.R., Martikainen, P.J. and Berggren, M. (2017) Degradation potentials of
554 dissolved organic carbon (DOC) from thawed permafrost peat. Sci. Rep. 7,
555 doi:10.1038/srep45811.
556 Spencer, R.G., Aiken, G.R., Wickland, K.P., Striegl, R.G. and Hernes, P.J. (2008)
557 Seasonal and spatial variability in dissolved organic matter quantity and composition
558 from the Yukon River basin, Alaska. Global Biogeochem. Cycles 22, doi:
559 10.1029/2008GB003231.
560 Spencer, R.G.M., Aiken, G.R., Butler, K.D., Dornblaser, M.M., Striegl, R.G. and
561 Hernes, P.J. (2009) Utilizing chromophoric dissolved organic matter measurements to
562 derive export and reactivity of dissolved organic carbon exported to the Arctic Ocean:
563 a case study of the Yukon River, Alaska. Geophys. Res. Lett. 36, 141-153.
564 Spencer, R.G.M., Guo, W., Raymond, P.A., Dittmar, T., Hood, E., Fellman, J. and
565 Stubbins, A. (2014) Source and biolability of ancient dissolved organic matter in glacier
566 and lake ecosystems on the Tibetan Plateau. Geochim. Cosmochim. Acta 142, 64-74.
567 Stenson, A.C.; Marshall, A.G.; Cooper, W.T., (2003) Exact masses and chemical
568 formulas of individual Suwannee River fulvic acids from ultrahigh resolution
569 electrospray ionization Fourier transform ion cyclotron resonance mass spectra, Anal.

570 Chem. 75, 1275-1284.
571 Striegl, R.G., Dornblaser, M.M., Aiken, G.R., Wickland, K.P. and Raymond, P.A. (2007)
572 Carbon export and cycling by the Yukon, Tanana, and Porcupine rivers, Alaska, 2001–
573 2005. Water Resour. Res. 43, doi:10.1029/2006WR005201.
574 Stubbins, A. and Dittmar, T. (2015) Illuminating the deep: Molecular signatures of
575 photochemical alteration of dissolved organic matter from North Atlantic Deep Water.
576 Mar. Chem. 177, 318-324.
577 Stubbins, A., Mann, P.J., Powers, L., Bittar, T.B., Dittmar, T., McIntyre, C.P., Eglinton,
578 T.I., Zimov, N. and Spencer, R.G.M. (2017) Low photolability of yedoma permafrost
579 dissolved organic carbon. J. Geophys. Res. Biogeosci. 122, 200-211.
580 Stubbins, A., Spencer, R.G.M., Chen, H.M., Hatcher, P.G., Mopper, K., Hernes, P.J.,
581 Mwamba, V.L., Mangangu, A.M., Wabakanghanzi, J.N. and Six, J. (2010) Illuminated
582 darkness: Molecular signatures of Congo River dissolved organic matter and its
583 photochemical alteration as revealed by ultrahigh precision mass spectrometry. Limnol.
584 Oceanogr. 55, 1467-1477.
585 Stuiver, M. and Reimer, P.J. (1993) Extended ^{14}C Data Base and Revised Calib 3. 0 14C
586 Age Calibration Program. Radiocarbon 35, 215-230.
587 Tarnocai, C., Canadell, J.G., Schuur, E.A.G., Kuhry, P., Mazhitova, G. and Zimov, S.
588 (2009) Soil organic carbon pools in the northern circumpolar permafrost region. Global
589 Biogeochem. Cycles 23, doi:10.1029/2008gb003327.
590 Vonk, J.E., Mann, P.J., Davydov, S., Davydova, A., Spencer, R.G.M., Schade, J.,
591 Sobczak, W.V., Zimov, N., Zimov, S., Bulygina, E., Eglinton, T.I. and Holmes, R.M.
592 (2013) High biolability of ancient permafrost carbon upon thaw. Geophys. Res. Lett.
593 40, 2689-2693.
594 Vonk, J.E., Tank, S.E., Bowden, W.B., Laurion, I., Vincent, W.F., Alekseychik, P.,

595 Amyot, M., Billet, M.F., Canario, J., Cory, R.M., Deshpande, B.N., Helbig, M., Jammet,
596 M., Karlsson, J., Larouche, J., MacMillan, G., Rautio, M., Anthony, K.M.W. and
597 Wickland, K.P. (2015) Reviews and syntheses: Effects of permafrost thaw on Arctic
598 aquatic ecosystems. Biogeosciences 12, 7129-7167.
599 Wang, B., Bao, Q., Hoskins, B., Wu, G. and Liu, Y. (2008) Tibetan Plateau warming
600 and precipitation changes in East Asia. Geophys. Res. Lett. 35, 63-72.
601 Wang, Y., Xu, Y., Spencer, R.G.M., Zito, P., Kellerman, A., Podgorski, D., Xiao, W.,
602 Wei, D., Rashid, H. and Yang, Y. (2018) Selective leaching of dissolved organic matter
603 from alpine permafrost soils on the Qinghai-Tibetan Plateau. J. Geophys. Res.
604 Biogeosci., 123, 1005-1016.
605 Ward, C. P. and Cory, R. M.(2015) Chemical composition of dissolved organic matter
606 draining permafrost soils. Geochim. Cosmochim. Acta 167, 63-79.
607 Ward, C.P. and Cory, R.M. (2016) Complete and Partial Photo-oxidation of Dissolved
608 Organic Matter Draining Permafrost Soils. Environ. Sci. Technol. 50, 3545-3553.
609 Weishaar, J.L., Aiken, G.R., Bergamaschi, B.A., Fram, M.S., Fujii, R. and Mopper, K.
610 (2003) Evaluation of specific ultraviolet absorbance as an indicator of the chemical
611 composition and reactivity of dissolved organic carbon. Environ. Sci. Technol. 37,
612 4702-4708.
613 Wickland, K.P., Aiken, G.R., Butler, K., Dornblaser, M.M., Spencer, R.G.M. and Striegl,
614 R.G. (2012) Biodegradability of dissolved organic carbon in the Yukon River and its
615 tributaries: Seasonality and importance of inorganic nitrogen. Global Biogeochem.
616 Cycles 26, doi:10.1029/2012GB004342.
617 Wild, B., Schnecker, J., Alves, R.J.E., Barsukov, P., Bárta, J., Čapek, P., Gentsch, N.,
618 Gittel, A., Guggenberger, G., Lashchinskiy, N., Mikutta, R., Rusalimova, O.,
619 Šantrůčková, H., Shibistova, O., Urich, T., Watzka, M., Zrazhevskaya, G. and Richter,

620 A. (2014) Input of easily available organic C and N stimulates microbial decomposition
621 of soil organic matter in arctic permafrost soil. Soil Biol. Biochem. 75, 143-151.
622 Wu, G., Liu, Y., Zhang, Q., Duan, A., Wang, T., Wan, R., Liu, X., Li, W., Wang, Z. and
623 Liang, X. (2007) The influence of mechanical and thermal forcing by the Tibetan
624 Plateau on Asian climate. J. Hydrometeorol. 8, 770-789.
625 Yao, T., Pu, J., Lu, A., Wang, Y. and Yu, W. (2007) Recent glacial retreat and its impact
626 on hydrological processes on the Tibetan Plateau, China, and surrounding regions. Arct.
627 Antarct. Alp. Res. 39, 642-650.
628 Zhang, Z.Q. and Wu, Q.-B. (2012) Predicting changes of active layer thickness on the
629 Qinghai-Tibet Plateau as climate warming. J. Glaciol. Geocryol. 34, 505-511.
630 Zhu, X., Wang, W. and Fraedrich, K. (2013) Future climate in the Tibetan Plateau from
631 a statistical regional climate model. J. Clim. 26, 10125-10138.
632 Zimov, S.A., Schuur, E.A.G. and Chapin, F.S. (2006) Permafrost and the global carbon
633 budget. Science 312, 1612-1613.
634
635

Figure and table captions

Fig. 1. Location of the QTP and sampling sites Q1 to Q20. Sites marked by a star were selected for FT-ICR MS and ^{14}C-DOC analyses. The AL and PL denote the sampling locations of the active and permafrost layers. The blue line and the red line represent the first order and second order stream, respectively, and the blue dashed line denotes stream without GPS data.

Fig. 2. (a) Stream water discharge, (b) pH, and (c) conductivity at the sampling sites in 2015; and (d) DOC concentration in stream water and PL/AL leachates collected in 2015 (filled circles) and 2016 (open circles).

Fig. 3. UV-visible optical indices of the stream water and PL/AL leachate samples collected in 2015 (filled circles) and 2016 (open circles) on the QTP: $S_{275\text{-}295}$ (a) and $SUVA_{254}$ (b).

Fig. 4. Variations of ^{14}C-DOC age across the alpine stream spatially (a), and at headstream Q-1 temporally (b).

Fig. 5. van Krevelen diagrams of AL leachate DOM (a), PL leachate DOM (b), headstream DOM Q-1 (c), downstream DOM Q-17 (d), the relative abundance of defined compound class in different samples (e). CA = condensed aromatics, Pol. = polyphenols, Uns. = highly unsaturated compounds, Ali. = aliphatics, Pep. = peptides; and Sug. = Sugar.

Fig. 6. (a) Relative contribution of AL leachate DOM to headstream DOM (Q-1); and (b) temporal variation of the DOC concentration at headstream Q-1.

Table 1 The number of molecular formulas assigned, modified aromaticity index (AI_{mod}), mean molecular weight (mean MW) and relative abundance of defined compound classes detected by FT-ICR MS for DOM samples from the QTP, including soil leachates (AL and PL) and stream waters (Q-1, Q-9 and Q-17). CA = condensed aromatics, Pol. = polyphenols, Uns. = highly unsaturated compounds, Ali. = aliphatic, Pep. = peptides.

Table 2 The number of specific molecules identified in the AL leachate DOM and the PL leachate DOM within the fluvial network, and the percentage of peaks totally degraded during the transportation.

Supplementary Figure S1. Van Krevelen diagrams showing the molecular changes of DOM from head to down-stream on the QTP. The blue and red dots denote decreasing trends and increasing trends, respectively. The color gradient shows the percentage of change. The lines separating compound categories [a]aliphatics and peptides [b] highly unsaturated compounds [c] polyphenols [d] condensed aromatics based on rules in the methods are just for visualization, and the exact categorization may differ.

674 Fig. 1

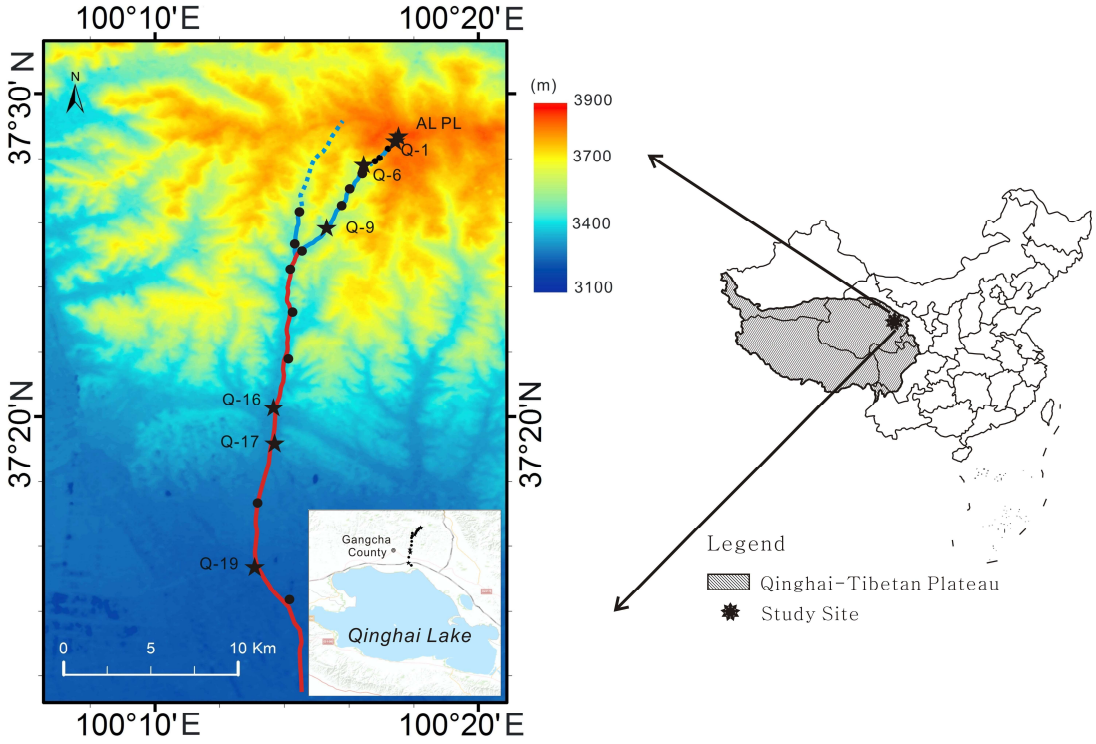

675

676

677 Fig. 2

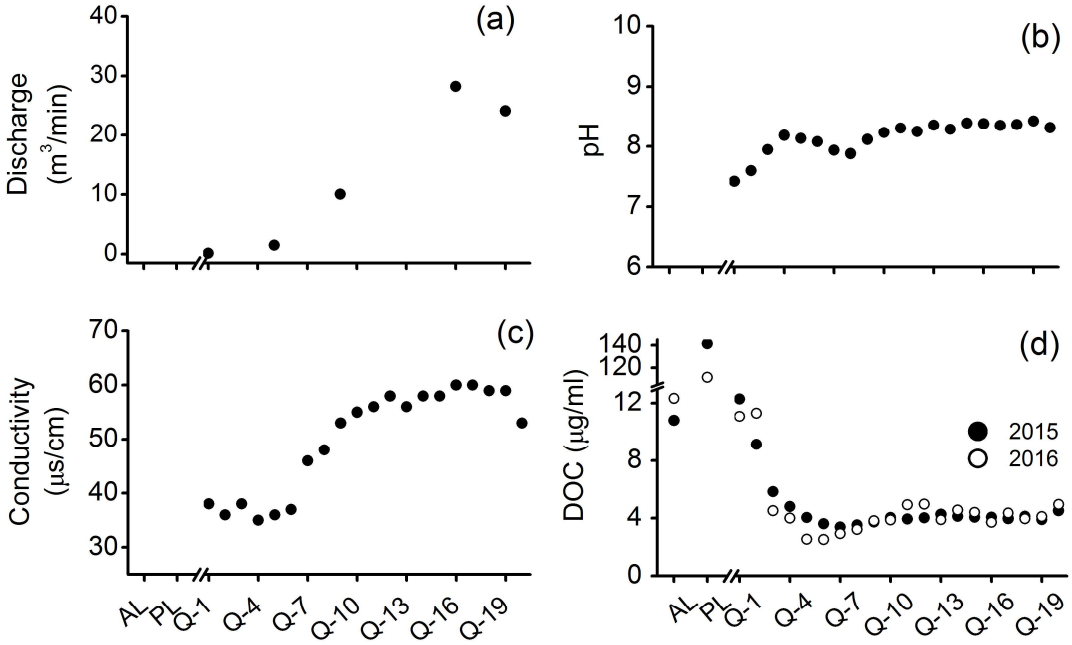

678

679

680 Fig. 3

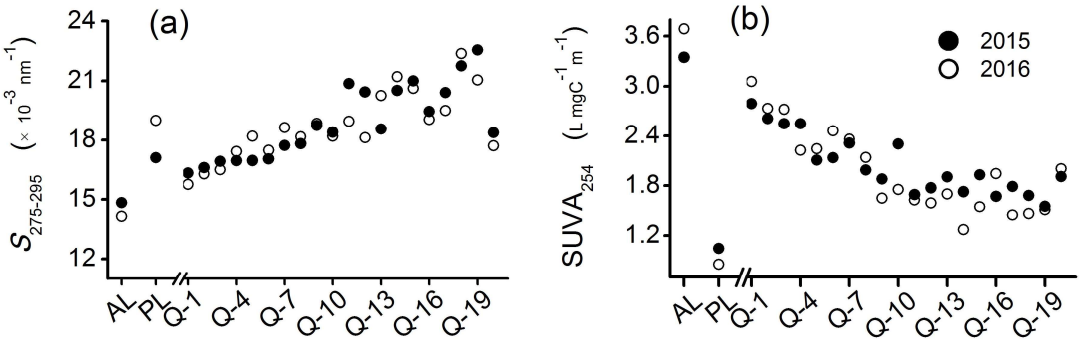

681

682

683 Fig. 4

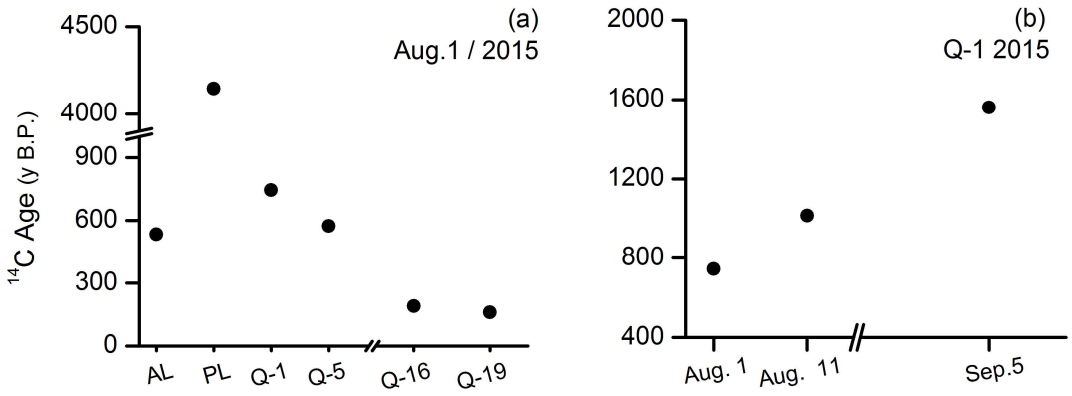

684

685

686 Fig. 5

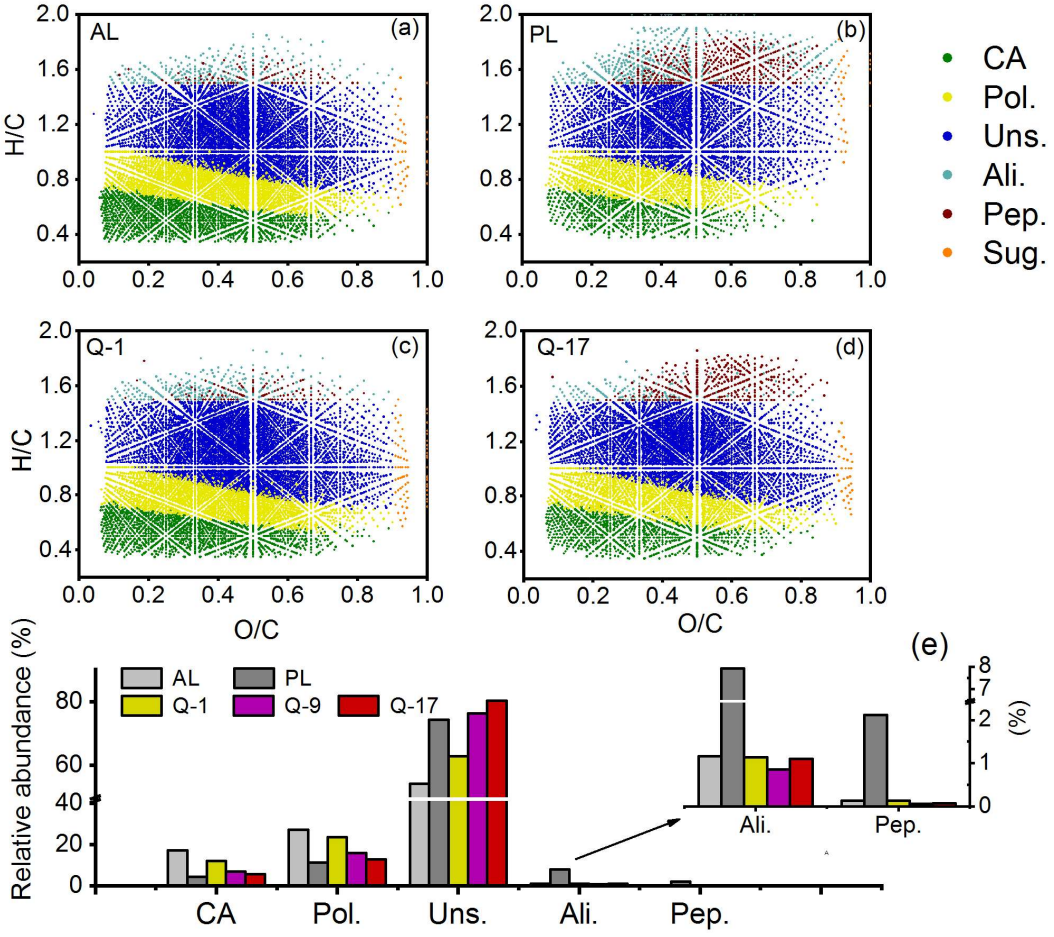

687

688

689 Fig. 6

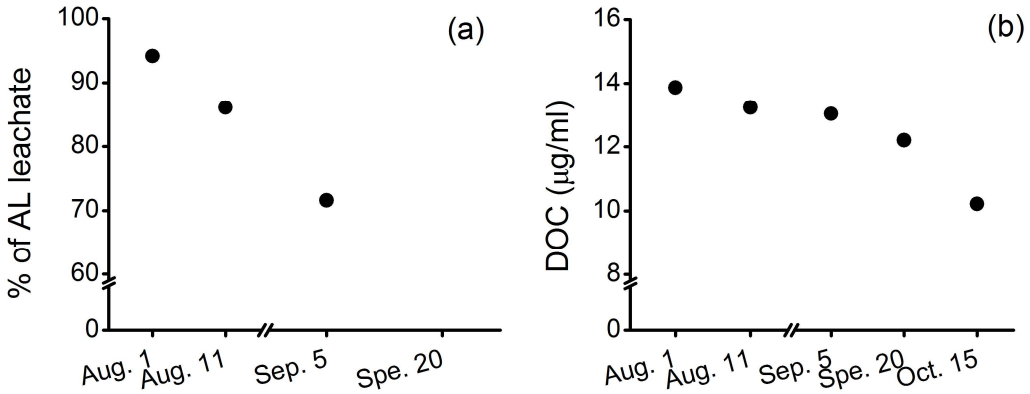

690

691

692 **Table 1.** The number of molecular formulas assigned, modified aromaticity index
693 (AI_{mod}), mean molecular weight (mean MW) and relative abundance of defined
694 compound classes detected by FT-ICR MS for DOM samples from the QTP, including
695 soil leachates (AL and PL) and stream waters (Q-1, Q-9 and Q-17). CA = condensed
696 aromatics, Pol. = polyphenols, Uns. = highly unsaturated compounds, Ali. = aliphatic,
697 Pep. = peptides.
698

Sample	Formulas assigned	Mean MW	AI_{mod}	CA (%)	Pol. (%)	Uns. (%)	Ali. (%)	Pep. (%)
AL	14709	498.81	0.47	17.23	27.10	54.28	1.16	0.14
PL	9645	452.73	0.30	4.32	11.33	74.23	7.92	2.12
Q-1	14924	510.07	0.43	12.05	23.69	62.85	1.14	0.14
Q-9	11724	500.19	0.38	6.86	15.82	76.32	0.86	0.06
Q-17	11074	486.50	0.36	5.53	12.91	80.31	1.11	0.08

699
700

Table 2: The number of specific molecules identified in the AL leachate DOM and the PL leachate DOM within the fluvial network, and the percentage of peaks totally degraded during the transportation.

Samples		All peaks	Only CHO	Contains N	Contains S	Contains N& S	Condensed aromatics	Polyhoenols	Unsatuated	Aliphatics	Peptides
AL specific	AL	6409	1793	3370	424	822	1620	1720	2970	38	23
	Q-1	5311 (17%)	1653 (8%)	2791 (17%)	349 (18%)	517 (37%)	1278 (21%)	1416 (18%)	2549 (14%)	20 (47%)	14 (39%)
	Q-9	3365 (47%)	1294 (28%)	1917 (43%)	153 (64%)	0 (100%)	748 (54%)	838 (51%)	1759 (41%)	6 (84%)	1 (96%)
	Q-17	2623 (59%)	985 (45%)	1570 (53%)	67 (84%)	0 (100%)	550 (66%)	602 (65%)	1453 (51%)	5 (87%)	0 (100%)
PL specific	PL	1345	515	551	278	0	2	23	318	597	385
	Q-1	222 (83%)	90 (83%)	102 (81%)	30 (89%)	0	0 (100%)	11 (52%)	126 (60%)	46 (92%)	36 (91%)
	Q-9	117 (91%)	44 (91%)	46 (92%)	27 (90%)	0	2 (0%)	14 (39%)	96 (70%)	1 (100%)	4 (99%)
	Q-17	130 (90%)	47 (91%)	55 (90%)	28 (90%)	0	2 (0%)	13 (43%)	104 (67%)	6 (99%)	5 (99%)

Figure S1.

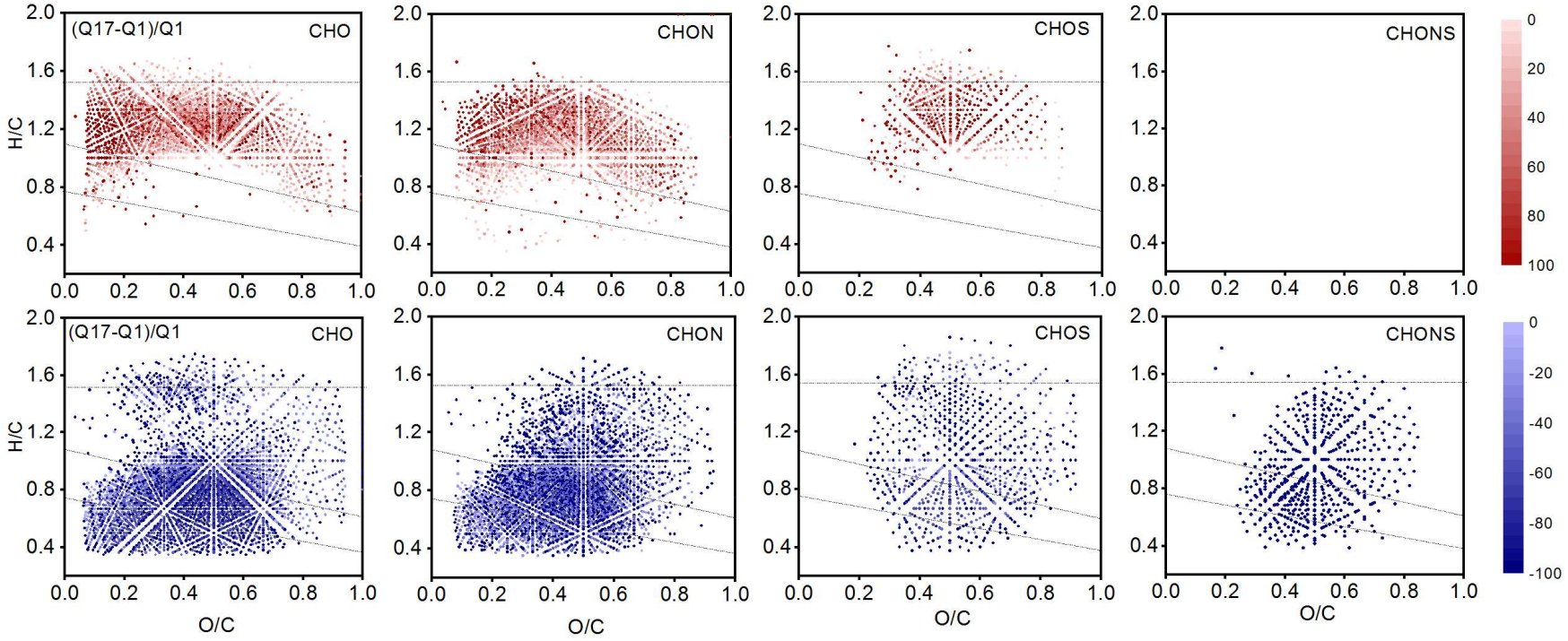
(Q17-Q1)/Q1
CHO
CHON
CHOS
CHONS
H/C
O/C
0
20
40
60
80
100
-20
-40
-60
-80
-100